Slot region electron loss timescales due to plasmaspheric hiss and lightning generated whistlers

Nigel P. Meredith,[1] Richard B. Horne,[1] Sarah A. Glauert,[1] and Roger R. Anderson,[2]

Roger R. Anderson, Department of Physics and Astronomy, University of Iowa, Iowa City, Iowa, IA 52242-1479. (roger-r-anderson@uiowa.edu)

Sarah A. Glauert, Richard B. Horne and Nigel P. Meredith, British Antarctic Survey, Natural Environment Research Council, Madingley Road, Cambridge, CB3 0ET, England. (sagl@bas.ac.uk; r.horne@bas.ac.uk; nmer@bas.ac.uk)

[1]British Antarctic Survey, Natural Environment Research Council, Cambridge, England

[2]Department of Physics and Astronomy, University of Iowa, Iowa City, USA.

Abstract.

Energetic electrons ($E > 100$ keV) in the Earth's radiation belts undergo Doppler-shifted cyclotron resonant interactions with a variety of whistler mode waves leading to pitch angle scattering and subsequent loss to the atmosphere. In this study we assess the relative importance of plasmaspheric hiss and lightning-generated whistlers in the slot region and beyond. Electron loss timescales are determined using the PADIE code with global models of the spectral distributions of the wave power based on CRRES observations. Our results show that plasmaspheric hiss propagating at small and intermediate wave normal angles is a significant scattering agent in the slot region and beyond. In contrast, plasmaspheric hiss propagating at large wave normal angles and lightning generated whistlers do not contribute significantly to radiation belt loss. The loss timescale of 2 MeV electrons due to plasmaspheric hiss propagating at small and intermediate wave normal angles in the centre of the slot region ($L = 2.5$) lies in the range 1-10 days, consistent with recent SAMPEX observations. Wave turbulence in space, which is responsible for the generation plasmaspheric hiss, thus leads to the formation of the slot region. During active periods losses due to plasmaspheric hiss may occur on a timescale of 1 day or less for a wide range of energies, 200 keV $< E <$ 1 MeV, in the region $3.5 < L < 4.0$. Plasmaspheric hiss may thus also be a significant loss process in the inner region of the outer radiation belt during magnetically disturbed periods.

1. Introduction

Relativistic electrons ($E > 1$ MeV) in the Earth's radiation belts are usually confined to two distinct zones. The inner radiation belt, which lies in the region $1.2 < L < 2.0$, is relatively stable. In contrast, the outer radiation belt, which lies in the region $3.0 < L < 7.0$, varies dramatically, particularly during enhanced geomagnetic activity [*Paulikas and Blake*, 1979; *Baker et al.*, 1986, 1994, 1997; *Li et al.*, 1997; *Reeves et al.*, 1998]. This variability is caused by an imbalance between source, transport and loss processes, all of which become enhanced during geomagnetic storms [*Horne*, 2002; *Summers et al.*, 2004; 2007a; *Thorne et al.*, 2005; *Horne et al.*, 2006]. Understanding this variability is important since enhanced fluxes of relativistic electrons damage spacecraft [*Wrenn*, 1995; *Baker*, 2001; *Wrenn et al.*, 2002] and are a risk to humans in space. Indeed, as society becomes ever more reliant on its assets in space, there is an increasing need to improve our knowledge of the processes governing the behaviour of these so-called "killer" electrons.

The slot region ($2.0 < L < 3.0$), that usually separates the inner ($1.3 < L < 2.0$) and outer ($3.0 < L < 7.0$) radiation belts, forms as the result of a balance between inward radial diffusion and pich angle scattering loss [*Lyons and Thorne*, 1973]. However, during major geomagnetic storms, such as the Halloween storm in 2003, the flux of relativistic electrons in the slot region increases dramatically [*Baker et al.*, 2004], as a result of enhanced inward transport and wave acceleration [*Horne et al.*, 2005; *Shprits et al.*, 2006; *Thorne et al.*, 2007]. The enhanced flux of relativistic electrons subsequently decay to the pre-storm equilibrium levels on a timescale of days to weeks, largely due to the resonant pitch angle scattering by plasmaspheric hiss [*Lyons et al.*, 1972; *Lyons and Thorne*, 1973;

Albert 1994; *Abel and Thorne* 1998a, 1998b], although losses due to lightning-induced electron precipitation may be important at lower energies [*Voss* et al., 1998; *Blake et al.*, 2001; *Rodger et al.*, 2002]. Further out pitch angle scattering by plasmaspheric hiss contributes to the loss of outer radiation belt electrons during the main and recovery phases of a storm [*Summers et al.*, 2007a] and can explain the quiet-time decay of outer radiation belt electrons over a wide range of energies and L shells [e.g., *Meredith et al.*, 2006a].

Plasmaspheric hiss is a broadband, structureless, whistler mode emission that is observed in the frequency range from 100 Hz to several kHz. Plasmaspheric hiss is observed in high density regions associated with the plasmasphere [*Dunckel and Helliwell*, 1969; *Russell et al.*, 1969; *Thorne et al.*, 1973] and plasmaspheric plumes [*Chan and Holzer*, 1976; *Cornilleau-Wehrlin et al.*, 1978; *Parrot and Lefeuvre*, 1986]. Plasmaspheric hiss intensifies during storms and substorms but can also persist during relatively quiet conditions [*Smith et al.*, 1974; *Thorne et al.*, 1974; 1977; *Meredith et al.*, 2004]

There are two leading theories for the origin of plasmaspheric hiss, in situ amplification of wave turbulence in space [e.g., *Thorne et al.*, 1973; 1979; *Church and Thorne*, 1983; *Huang et al.*, 1983; *Thorne and Barfield*, 1976; *Solomon et al.*, 1988; *Cornilleau-Wehrlin et al.*, 1993] and lightning generated whistlers [e.g., *Dowden*, 1971; *Draganov et al.*, 1993; *Bortnik et al.*, 2003]. Although lightning generated whistlers are impulsive, after several magnetospheric reflections, dispersion, and mixing with other lightning generated whistlers, it is postulated that they merge into a broadband signal that becomes plasmaspheric hiss [*Dowden*, 1971; *Draganov et al.*, 1993; *Bortnik et al.*, 2003].

Green et al., [2005] recently analysed data from DE1 and IMAGE and showed that the distribution of the wave emissions at 3 kHz is similar to the distribution of lightning in geographic longitude, namely that the emissions are stronger over the continents than the ocean. They stated that the correspondence between the enhanced intensities and the continents occurs over the frequency range $0.5 < f < 3.0$ kHz and concluded that lightning is the dominant source of plasmaspheric hiss. This interpretation has been disputed [see the comment by *Thorne et al.*, 2006 and the reply by *Green et al.*, 2006]. *Meredith et al.* [2006b] subsequently analysed the longitudinal distribution of the wave intensities over the frequency range $0.1 < f < 5.0$ kHz using data from the CRRES satellite. They found that the waves at higher frequencies ($2.0 < f < 5.0$ kHz) are most likely related to lightning generated whistlers, consistent with the *Green et al.*, [2005] results at 3 kHz. However, in sharp contrast to the higher frequency waves, they found that the waves at lower frequencies ($0.1 < f < 2.0$ kHz) are independent of lightning activity, are stronger on the dayside, and increase with geomagnetic activity. This suggests that wave turbulence in space, generated by plasma instabilities, is responsible for the bulk of the wave power between 100 Hz and 2 kHz. Furthermore, the wave intensities are an order of magnitude or more higher at the lower frequencies [*Meredith et al.*, 2006b]. Since electron loss, via pitch angle scattering into the loss cone, is proportional to the wave power, this suggests that natural turbulence could be responsible for the formation of the slot region.

The purpose of this paper is to take into account the different generation mechanisms of the plasmaspheric wave emissions and assess their relative roles in the loss of energetic electrons. In this study we split the plasmaspheric wave emissions into two wave bands, the low frequency waves ($0.1 < f < 2.0$ kHz) for which there is strong evidence for generation by plasma instabilities in space, and the high frequency waves ($2.0 < f < 5.0$ kHz) which are most likely generated by lightning in thunderstorms as lightning generated whistlers. Although lightning generated whistlers may contribute to the low frequency band, our observations suggest that the low frequency band is dominated by waves generated by wave turbulence in space [*Meredith et al.*, 2006b]. Similarly, waves generated by wave turbulence in space may occur in the high frequency band, but our observations suggest that the high frequency band has a significant contribution from lightning generated whistlers. We henceforth refer to the low frequency band as plasmaspheric hiss, and the high frequency band as lightning generated whistlers. We model the distribution of the wave power in these two bands and use the PADIE code to determine their relative importance for electron loss in the slot region and beyond.

2. Instrumentation

The wave data used in this study were provided by the Plasma Wave Experiment on board CRRES. This satellite, which was launched on 25 July 1990, operated in a highly elliptical geosynchronous transfer orbit with a perigee of 305 km, an apogee of 35,768 km and an inclination of 18^o. The orbital period was approximately 10 hours, and the initial apogee was at a magnetic local time (MLT) of 0800 MLT. The magnetic local time of apogee decreased at a rate of approximately 1.3 hours per month until the satellite failed on 11 October 1991, when its apogee was at about 1400 MLT. The satellite covered a range of L shells from $L = 1.05$ to $L = \sim 8$ and a range of magnetic latitudes within $\pm 30^o$ of the magnetic equator, sweeping through the radiation belts approximately 5 times per day, providing good coverage of this important region for almost 15 months.

The Plasma Wave Experiment provided measurements of electric fields from 5.6 Hz to 400 kHz, using a 100 m tip-to-tip long wire antenna, with a dynamic range covering a factor of at least 10^5 in amplitude [*Anderson et al.*,1992]. The sweep frequency receiver covered the frequency range from 100 Hz to 400 kHz in four bands with 32 logarithmically spaced steps per band, the fractional step separation, Δ f/f, being about 6.7% across the entire frequency range.

3. Data Analysis

3.1. Determination of the Characteristic Frequencies

The local electron gyrofrequency, f_{ce}, is determined directly from the fluxgate magnetometer onboard the spacecraft [*Singer et al.*, 1992]. The equatorial electron gyrofrequency, $f_{ce,eq}$, is subsequently determined from the local gyrofrequency assuming a dipole field:

$$f_{ce,eq} = f_{ce} L^3 \cos^6 \lambda_m / \sqrt{(1 + 3 \sin^2 \lambda_m)} \quad (1)$$

where λ_m is the magnetic latitude.

Inside the plasmasphere emissions at the upper hybrid resonance frequency, f_{uhr} are usually well-defined and the electron plasma frequency, f_{pe}, is determined from measurements of f_{uhr} using the relationship $f_{pe}^2 = f_{uhr}^2 - f_{ce}^2$. Beyond the plasmapause f_{pe} is determined from the lower frequency limit of the electromagnetic continuum radiation which is taken to be a plasma wave cut off at the plasma frequency [*Gurnett and Shaw*, 1973].

Inside $L = 3$ the plasma frequency, and consequently the upper hybrid frequency, can exceed 400 kHz which is the upper frequency limit of the sweep frequency receiver. In these circumstances we apply a correction when the observations at $L = 3$ are inside the plasmapause by assuming that the radial density profile in the plasmasphere is represented by an L^{-4} distribution [*Chappel et al.* 1970]. In this case, the plasma frequency, f_{pe}, scales as L^{-2}. Therefore, when f_{uhr} exceeds 400 kHz at a given L, $(L < 3)$ and the measurement at $L = L_0 = 3.0$ is in the plasmasphere, we estimate $f_{pe}(L)$ using the derived plasma frequency at L_0, $f_{pe}(L_0)$, using:

$$f_{pe}(L) = L_0^2 f_{pe}(L_0)/L^2 \quad (2)$$

3.2. Wave Database

The wave data are initially corrected for the instrumental background response and smoothed by using a running 3 minute average to take out the beating effects due to differences in the sampling and the spin rate. Spurious data points, data spikes, and periods of instrumental downtime are flagged and ignored in the subsequent statistical analyses. Twelve orbits, during which nontraditional configurations were deployed for testing purposes, are also excluded from the analyses.

Since pitch angle diffusion rates scale as the magnetic field intensity the electric field spectral intensities, S_E, are converted to magnetic field spectral intensities, S_B, using the expression:

$$S_B = \frac{1}{c^2}\left(1 + \frac{f_{pe}^2}{f(f_{ce} - f)}\right) S_E \quad (3)$$

derived from Maxwell's 3 rd equation and the cold plasma dispersion relation for whistler mode waves assuming that the direction of propagation of the waves is parallel to the ambient magnetic field. Here c is the speed of light and f is the wave frequency. The wave magnetic field intensities for plasmaspheric hiss and lightning generated whistlers are subsequently determined by integrating the wave magnetic field spectral intensities over the frequency range $0.1 < f < 2.0$ and $2.0 < f < 5.0$ kHz respectively.

The wave magnetic field spectral intensity in $\mathrm{pT^2Hz^{-1}}$ in each frequency channel, together with the wave magnetic field intensities of plasmaspheric hiss and lightning generated whistlers in $\mathrm{pT^2}$, the ratio $f_{pe}/f_{ce,eq}$ and the electric field intensities between $f_{ce} < f < 2f_{ce}$, are rebinned as a function half-orbit (outbound and inbound) and L in steps of $0.1L$. The universal time (UT), magnetic latitude (λ_m), magnetic local time (MLT), and time spent in each bin are also recorded at the same resolution. The resulting database, consisting of measurements from 939 orbits (1878 half-orbits), is subsequently analysed to determine the average wave spectral profiles over the frequency range $0.1 < f < 5.0$ kHz as a function of L shell and geomagnetic activity.

3.3. Identification of Plasmaspheric Hiss and Lightning Generated Whistlers

The database of wave emissions in the frequency range between 0.1 and 5.0 kHz may contain other wave modes in addition to plasmaspheric hiss and lightning generated whistlers. These other wave modes are carefully removed from the database as described below.

Whistler-mode chorus waves, which are observed in the low-density region outside of the plasmapause, can fall into the frequency range between 0.1 and 5 kHz [e.g. *Meredith et al.*, 2001]. In order to exclude these emissions from the study we adopt a criterion based on the amplitude of the waves in the band $f_{ce} < f < 2f_{ce}$. Waves in this frequency band, which contain contributions from both electron cyclotron harmonic waves and thermal noise, tend to be excluded from the high density region inside the plasmapause. Specifically we adopt the criterion, based on a previous experimental study using data from the CRRES Plasma Wave Experiment, that the wave amplitude for frequencies in the range $f_{ce} < f < 2f_{ce}$ must be less than 0.0005 mVm^{-1} in order for wave emissions in the frequency range $0.1 < f < 5$ kHz to be included in the survey [*Meredith et al.*, 2004]. This criterion naturally restricts the study to the plasmasphere which is the region where the vast majority of plasmaspheric hiss and lightning generated whistlers are observed.

Magnetosonic waves, which are observed in the inner magnetosphere at frequencies below the lower hybrid resonance frequency, may also fall into the frequency range between 0.1 and 5 kHz. *Gurnett* [1976] analysed equatorial crossings in the region $2 < L < 3.5$ and found that the waves were largely confined to within 5^o of the magnetic equatorial plane. These waves are excluded from our survey by excluding emissions observed within $\pm 5^o$ of the magnetic equator.

4. Calculation of Electron Loss Timescales

We investigate the relative roles of plasmaspheric hiss and lightning generated whistlers as loss processes using wave observations from the CRRES spacecraft to calculate the pitch-angle diffusion rates for electrons. The diffusion rates are calculated using the PADIE (Pitch Angle and energy Diffusion of Ions and Electrons) code [*Glauert and Horne*, 2005].

Since resonant scattering by hiss is not sensitive to the ion composition an electron/proton plasma is assumed. The determination of the diffusion coefficients then requires knowledge of the distribution of the wave power spectral density with frequency and wave normal angle, together with the ratio f_{pe}/f_{ce}, wave mode, and the number of resonances. We calculate the bounce-averaged pitch-angle diffusion coefficients for whistler mode hiss by summing the contributions from the n = -5 to n = +5 cyclotron harmonic resonances and the Landau resonance (n = 0).

The waves are assumed to have a Gaussian frequency distribution given by:

$$B^2(\omega) = \begin{cases} A^2 \exp\left(-\left(\frac{\omega-\omega_m}{\delta\omega}\right)^2\right) & \omega_{lc} \leq \omega \leq \omega_{uc} \\ 0 & \text{otherwise,} \end{cases} \tag{4}$$

where B^2 is the power spectral density of wave magnetic field (in $\mathrm{T}^2\ \mathrm{Hz}^{-1}$), ω_m and $\delta\omega$ are the frequency of maximum wave power and bandwidth, respectively, ω_{lc} and ω_{uc} are lower and upper bounds to the wave spectrum outside which the wave power is zero, and A^2 is a normalization constant given by

$$A^2 = \frac{|B_w|^2}{\delta\omega} \frac{2}{\sqrt{\pi}} \left[\mathrm{erf}\left(\frac{\omega_m - \omega_{lc}}{\delta\omega}\right) + \mathrm{erf}\left(\frac{\omega_{uc} - \omega_m}{\delta\omega}\right)\right]^{-1} \tag{5}$$

where B_w is the wave amplitude in units of Tesla. The distribution of wave normal angles ψ is also assumed to be Gaussian, given by

$$g(X) = \begin{cases} \exp\left(-\left(\frac{X-X_m}{\delta X}\right)^2\right) & X_{lc} \leq X \leq X_{uc} \\ 0 & \text{otherwise,} \end{cases} \tag{6}$$

where $X = \tan(\psi)$, δX is the angular width, X_m is the peak, and X_{lc} and X_{uc} are the lower and upper bounds to the wave normal distribution outside of which the wave power is zero.

Once the pitch-angle diffusion rates are calculated, the timescale for the electrons to pitch-angle scatter into the loss cone can be determined. We assume that the electron distribution function satisfies the one-dimensional pitch-angle diffusion equation and can be factorised into time-dependent and pitch-angle dependent functions [*Lyons et al.*, 1972; *Albert* 1994]. The resulting equation can be cast as a two-point boundary value problem in 4 variables [*Albert,* 1994], and solved to obtain the loss timescale, τ [*Meredith et al.*, 2006a].

4.1. Model of the Wave Power

Energetic electrons ($E > 100$ keV) in the Earth's outer radiation belt drift around the Earth on timescales of the order of hours or less which means that they typically complete many orbits during their lifetime. We thus require a global model of the wave spectral intensities to obtain an estimate of the loss timescales.

Global statistical models of the average intensities of plasmaspheric hiss and lightning generated whistlers are shown as a function of L and MLT for different levels of geomagnetic activity in Figure 1. From left to right models are presented for quiet ($AE^* < 100$ nT), moderate ($100 < AE^* < 500$ nT), and active ($AE^* > 500$ nT) conditions. Here AE^* is the maximum value of the AE index in the previous 3 hours [*Meredith et al.*, 2004]. The average intensities are shown in the large panels and the corresponding sampling distributions are in the small panels. Plasmaspheric hiss (bottom) is present during quiet times but intensifies during moderate and active conditions consistent with previous work [*Meredith et al.*, 2004]. The waves peak on the dayside during active conditions with intensities typically of the order of 3000 pT^2. Lightning generated whistlers (top) tend to be an order of magnitude or more less intense than plasmaspheric hiss over the entire region and during all conditions. In the region $2 < L < 3$ lightning generated whistlers are strongest in the evening sector. They also increase with increasing geomagnetic activity which suggests that the lightning generated waves may be further amplified by wave particle interactions in space. Further out, in the region $3 < L < 4$ a second population of stronger waves are observed during moderate and active conditions on the dayside. These waves, which are substorm-dependent, are unlikely to be related to lightning generated whistlers since D region attenuation maximises on the dayside and the lightning activity is weakest in the morning sector. This suggests that waves generated by wave turbulence in space can extend to higher frequencies and that waves classified as lightning-generated whistlers may contain a contribution from natural instabilities. However, since the frequency range from 2 - 5 kHz includes lightning generated waves [*Meredith et al.*, 2006b], we can use this band to estimate a lower limit on the loss timescales due to lightning generated whistlers.

To assess the frequency distribution of the waves we determine the average wave magnetic field spectral intensities inside the plasmasphere as a function of frequency, L shell and geomagnetic activity. We average the wave spectral intensities first over the magnetic latitude range $5^o < |\lambda_m| < 30^o$ and then over magnetic local time. The resulting spectral intensities (black traces) are plotted as a function of frequency in Figure 2. The spectral intensities are shown for quiet (top) and active (bottom) conditions for, from left to right, $L = 2.0$ to $L = 4.0$ in steps of $0.5L$. The vertical dashed line at 2 kHz divides the frequency range into plasmaspheric hiss (to the left) and lightning generated whistlers (to the right). In all cases the wave spectral intensity maximises at low frequencies and subsequently decreases with increasing frequency. The bulk of the wave power in the region $2.0 < L < 4.0$ is clearly associated with plasmaspheric hiss, during both quiet and active conditions. The PADIE code requires the frequency distribution of the waves to be modelled as a Gaussian or series of Gaussian distributions. We find that three Gaussian profiles are needed to provide a good fit to the entire frequency range. The first component (red) is a least squares fit to plasmaspheric hiss at low frequencies and has an upper cut-off at the frequency where the fit departs from the data. The second component (orange) is a least squares fit to plasmaspheric hiss from the upper cut-off of the first component to 2 kHz and the third component (green) is a least squares fit to the lightning generated whistlers. Since the second and third components do not possess a peak in their spectral intensities we fix the peak frequency at 0.1 Hz. The fits can be seen to represent the data well over almost the entire frequency range for all activities and L shells. Details of the fitting parameters are shown in Tables 1 and 2 for quiet and active conditions respectively. Here $f_{0,x}$, df_x, and $B^2_{w,x}$ represent the peak frequency in Hz, the frequency bandwidth in Hz, and the wave intensity in pT^2 of the x^{th} Gaussian component.

Since plasmaspheric hiss is observed throughout the plasmasphere [e.g. *Thorne et al.*, 1973], we assume the average wave spectral profiles from $5^o < |\lambda_m| < 30^o$ are representative of the emissions at all latitudes. We then calculate the bounce-average diffusion rate which takes into account the scattering of particles in pitch angle over the complete range of latitudes between the particle's mirror points. In general the waves resonate with higher energy electrons at higher latitudes and will tend to scatter higher energy electrons into the loss cone at higher latitudes. This is shown in more detail in Figure 2 of *Horne and Thorne* [2003] for the case of chorus waves.

4.2. Wave Normal Models

Plasmaspheric hiss appears to propagate over a broad range of wave normal angles with predominantly field-aligned propagation near the geomagnetic equator and more oblique propagation at higher latitudes. [*Parrot and Lefeuvre*, 1986; *Hayakawa et al.*, 1986; *Santolik et al.*, 2001]. For example, in the equatorial region ($\lambda_m < 10^o$) *Parrot and Lefeuvre*, [1986] found two populations of wave normal angles one lying in the range $0^o \leq \psi \leq 30^o$, the other in the range $40^o \leq \psi \leq 60^o$. At higher latitudes ($\lambda_m > 20^o$) most of the waves had larger wave normal angles in the range $55^o \leq \psi \leq 85^o$. To investigate the effect of the wave normal angle on the precipitation lifetimes we use three different angular distributions of hiss, chosen to be representative of these observations [Table 3].

Lightning generated whistlers guided along the magnetic field by ducts of enhanced plasma density for $f < 0.5f_{ce}$ (and density depletions for $f > 0.5f_{ce}$) propagate at small wave normal angles [*Smith*, 1961]. Unducted lightning generated whistlers that exit the ionosphere at low latitudes may propagate to the slot region and beyond following many magnetospheric reflections. The wave normal angle of magnetospherically reflected (MR) whistlers rapidly increase towards $\psi = 90^o$ at the first reflection. The waves subsequently remain highly oblique [e.g., *Thorne and Horne*, 1994]. We, therefore, adopt the small and large wave normal models to investigate the role of ducted and MR whistlers respectively [Table 3].

The conversion from electric field intensity to magnetic field intensity assumes parallel propagation [*Meredith et al.*, 2004]. We calculate approximate intensities for propagation at 52^o and 80^o using the cold plasma dispersion solver in the HOTRAY code [*Horne*, 1989] assuming a frequency of 0.4 kHz and 0.7 kHz for the two components of plasmaspheric hiss and a frequency of 2.0 kHz for lightning generated whistlers. These frequencies are chosen since, for each component, they roughly correspond to the frequencies where the wave power peaks. The wave intensities for plasmaspheric hiss for the three wave normal models, and the ducted and MR whistlers are plotted as a function of L shell in Figure 3. The results are presented for both quiet (left) and active (right) conditions. Plasmaspheric hiss (red) is typically one or two orders of magnitude more intense than the lightning generated whistlers (blue) during both quiet and active conditions. The wave intensity for plasmaspheric hiss propagating parallel to the magnetic field (red, solid) is typically factors of 1.5 and 6 higher than for plasmaspheric hiss propagating at 52^o (red, dashed) and 80^o (red, dotted) respectively. Ducted whistlers (blue, solid) are about a factor of 4 more intense than MR whistlers in the region $2.0 < L < 3.5$. For each wave normal angle considered plasmaspheric hiss is typically a factor of 3 more intense during active conditions. At low L ($2.0 < L < 2.5$) lightning generated whistlers are up to a factor of 2 more intense during active conditions. Further out the wave intensities increase by a factor of 10 or more and are due to the appearance of the second population of waves in this frequency range noted above.

4.3. Model of $f_{pe}/f_{ce,eq}$

The mean value of the ratio of $f_{pe}/f_{ce,eq}$ is plotted as a function of L shell and MLT for different levels of geomagnetic activity in the top panels of Figure 4. From left to right the results are shown for quiet, moderate, and active conditions. The ratios are shown in the large panels and the sampling distributions in the small panels. $f_{pe}/f_{ce,eq}$ ranges from ∼5 at the inner edge of the slot region to ∼15 near geostationary orbit. During active conditions the plasmasphere is compressed, particularly on the dawnside as evidenced by the sampling distribution of the measurements inside the plasmasphere. For measurements inside the plasmasphere the average values of $f_{pe}/f_{ce,eq}$ at any given location tend to be slightly less than during quiet conditions. Line plots of the ratio $f_{pe}/f_{ce,eq}$ are plotted as a function of MLT for specified L shells for quiet, moderate, and active conditions in the bottom panels of Figure 3. The solid lines, colour-coded to denote the L shell, represent the data and the dashed lines indicate the average values. At each L shell the values typically lie within ±20% of the mean value and justify the use of the mean value in our calculations. The post-noon minimum seen in the region $3.0 < L < 4.0$

during moderate and active conditions is intriguing. This feature is caused by a sampling effect and is due to the occurrence of strong and persistent magnetic activity when the satellite was in this region, as evidenced by the concomitant poor sampling statistics for quiet conditions. The average values of $f_{pe}/f_{ce,eq}$ are plotted as a function of L shell in Figure 5. The average value of $f_{pe}/f_{ce,eq}$ increases approximately linearly with increasing L shell, in line with expectations since the equatorial magnetic field strength scales as L^{-3}, and the number density scales as L^{-4}. The average values of $f_{pe}/f_{ce,eq}$ during quiet conditions (blue) are typically ∼10% larger than during active conditions (red).

5. Electron Loss Timescales

The electron loss timescales due to plasmaspheric hiss (red) and lightning generated whistlers (blue) at $L = 2.5$ are shown as a function of energy (100 keV $< E <$ 5 MeV) for active conditions in Figure 6. The results for the small, intermediate, and large wave normal models are shown as solid, dashed and dotted lines respectively. The upper and lower black horizontal dotted lines represent loss timescales of 10 days and 1 day respectively. For energies greater than 500 keV the smallest loss timescales are due to plasmaspheric hiss propagating at small or intermediate wave normal angles and can be as low as ∼1 day at 2 MeV. The loss timescales for plasmaspheric hiss propagating at large wave normal angles are all greater than 500 days, indicating that these waves are relatively unimportant. At relativistic energies (E > 1 MeV) the loss timescales due to plasmaspheric hiss propagating at small and intermediate wave normal angles are an order of magnitude or more shorter than those due to ducted whistlers. However, at lower energies (E < 500 keV) ducted whistlers become a more effective scattering agent than plasmaspheric hiss but the loss timescales are long and greater than 100 days. The loss timescales for MR whistlers are insignificant at all energies.

We investigate the behaviour of the electron loss timescales as a function of energy at different L shells during active conditions in the bottom panels of Figure 7. From left to right the electron loss timescales are shown as a function of energy for $L = 2.0$ to $L = 4.0$ in steps of $0.5L$. At any given L shell the shortest loss timescales occur predominantly for plasmaspheric hiss propagating at small and intermediate wave normal angles. Moving out in L plasmaspheric hiss becomes increasingly effective over a wider range of energies. At $L = 2.0$ the loss timescales due to plasmaspheric hiss can be as low as 10 days at 5 MeV during active conditions but become prohibitively large at energies less than 2 MeV. At $L = 3.0$ the loss timescales are 1 - 10 days for waves propagating at small and intermediate wave normal angles over a wide range of energies (300 keV $< E <$ 3 MeV). Further out, the loss timescales due to plasmaspheric hiss propagating at small or intermediate wave normal angles can be significantly shorter than 1 day over a wide range of energies.

The loss timescales during quiet conditions are shown in the top panels of Figure 7. Once again, at any given L shell the shortest loss timescales occur predominantly for plasmaspheric hiss propagating at small and intermediate wave normal angles. Furthermore, moving out in L plasmaspheric hiss becomes increasingly effective over a wider range of energies. However, the loss timescales tend to be about an order of magnitude smaller during active conditions when compared to quiet conditions.

We investigate the behaviour of the electron loss timescales as a function of L shell at different energies during quiet and active conditions in the top and bottom panels of Figure 8 respectively. From left to right the electron loss timescales are shown as a function of L shell for energies ranging from 100 keV to 2 MeV. The loss timescales for electrons with energies of 100 keV fall below 10 days only in the inner region of the outer radiation belt ($3.5 < L < 4.0$). However, as the electron energy increases plasmaspheric hiss becomes more effective at lower L shells. For example, at 500 keV the loss timescales can be less than 10 days from $L = 3.0$ and beyond. At MeV energies plasmaspheric hiss is an effective scattering agent in both the slot region and beyond ($2.5 < L < 4.0$).

6. Discussion

The slot region ($2.0 < L < 3.0$) between the inner and outer radiation belt is usually devoid of relativistic electrons. However, during strong storms, the slot region can become filled [e.g., *Baker et al.*, 2004]. The slot region subsequently reforms on a timescale of days to weeks. For example, *Baker et al.* [2004], using SAMPEX data, estimated e-folding loss timescales of 4.6 and 2.9 days following enhancements of 2 - 6 MeV electrons at $L = 2.5$ in November 2003. At $L = 2.5$, the loss timescales of 2 MeV electrons due to plasmaspheric hiss range from 1-10 days depending on the level of geomagnetic activity (Figure 7) and are consistent with the SAMPEX findings.

At 1 MeV losses due to plasmaspheric hiss at $L = 2.5$ take place on slightly longer timescales of tens of days (Figure 7). These losses are solely due to plasmaspheric hiss propagating at small and intermediate wave normal angles. Plasmaspheric hiss propagating at large wave normal angles and lightning generated whistlers do not play a significant role. Since plasmaspheric hiss is caused by wave turbulence in space [*Meredith et al.*, 2006b], wave turbulence in space is responsible for the formation of the slot region.

At lower energies (E $<\sim$ 500 keV) at $L = 2.5$ both plasmaspheric hiss and lightning generated whistlers are ineffective (Figure 7). In this region and at these energies whistler mode waves from ground-based VLF transmitters, used for communication with submarines are likely to be the dominant loss mechanism [e.g., *Abel and Thorne*, 1998a].

During quiet times the loss timescales in the region $3.0 < L < 4.0$ lie in the range 3-10 days at 1 MeV (Figure 8), consistent with observations and previous estimates using the PADIE code with CRRES measurements of plasmaspheric hiss [*Meredith et al.*, 2006a]. At lower energies, 200 keV, the loss timescales can be faster than a day at $L = 4.0$ but rise to 5 days at $L = 3.5$ and become prohibitively large inside $L = 3.0$ (Figure 8).

If plasmaspheric hiss is to play an important role during active times then the timescale for loss must also be of the order of a few days or less. We see that this can occur in the inner part of the outer radiation belt ($3.5 < L < 4.0$) over the important energy range from $\sim$ 200 keV to $\sim$ 1 MeV (Figure 7). Plasmaspheric hiss could thus play an important role in the loss of energetic electrons in the region $3.5 < L < 4.0$ during magnetically disturbed periods. During active periods the plasmasphere tends to be restricted to the region inside $L = 4.0$, although hiss may also be present in plumes at higher L during these intervals. Indeed, recent modelling results suggest that plasmaspheric hiss can also effectively scatter energetic electrons in plumes [*Summers et al.*, 2007b].

Unducted lightning generated whistlers can form a population of magnetospherically reflected (MR) whistlers that remain geomagnetically trapped in the inner magnetosphere. It has been suggested that these waves could merge into a continuum with characteristic features similar to plasmaspheric hiss [*Dowden*, 1971; *Draganov et al.*, 1993; *Bortnik et al.*, 2003]. CRRES observations suggest that these waves make a significant contribution to the plasmaspheric emissions at high frequencies ($2.0 < f < 5.0$ kHz) but do not contribute significantly to the higher intensity emissions at lower frequencies ($0.1 < f <$

2.0 kHz) [*Meredith et al.*, 2006b]. Since MR whistlers propagate at large wave normal angles [*Thorne and Horne*, 1994], our present study confirms that they cannot play an important role in radiation belt electron loss.

7. Conclusions

We estimate loss timescales due to plasmaspheric hiss and lightning generated whistlers in the slot region and beyond using the PADIE code with CRRES wave data. Our principal results are as follows:

1. Plasmaspheric hiss propagating at small and intermediate wave normal angles is the dominant scattering agent of electrons with energies greater than 500 keV in the region $2.5 < L < 4.0$. Plasmaspheric hiss propagating at large wave normal angles and lightning generated whistlers do not contribute significantly to radiation belt loss.

2. The loss timescale of 2 MeV electrons due to plasmaspheric hiss in the centre of the slot region ($L = 2.5$) lies in the range 1-10 days, consistent with recent SAMPEX observations

3. The slot region at ∼MeV energies is caused by resonant wave particle interactions with plasmaspheric hiss. Since plasmaspheric hiss is produced by wave turbulence in space, the slot region is caused by wave turbulence in space and not lightning (as suggested by *Green et al.*, [2005]).

4. During active conditions losses due to plasmaspheric hiss may occur on a timescale of 1 day or less for 200 keV $< E <$ 1 MeV in the region $3.5 < L < 4.0$.

Plasmaspheric hiss, generated by wave turbulence in space, is an important loss mechanism both in the slot region and beyond. Indeed, plasmaspheric hiss may even be an important loss process in the inner region of the outer radiation belt during magnetically disturbed periods. Realistic, physics-based, models of the Earth's radiation belts, that are currently being developed to understand and ultimately predict the Earth's radiation environment, should thus include resonant wave-particle interactions with plasmaspheric hiss.

Acknowledgments. We thank the NSSDC Omniweb for providing the AE indices used in this paper. This work was supported by the National Environment Research Council.

References

Abel, B., and R. M. Thorne (1998a), Electron scattering loss in Earth's inner magnetosphere, 1. Dominant physical processes, *J. Geophys. Res., 103*, 2385.

Abel, B., and R. M. Thorne (1998b), Electron scattering loss in Earth's inner magnetosphere, 2. Sensitivity to model parameters, *J. Geophys. Res., 103*, 2397.

Albert, J. M. (1994), Quasi-linear pitch angle diffusion coefficients: Retaining high harmonics, *J. Geophys. Res., 99*, 23,741.

Anderson, R. R., D. A. Gurnett, and D. L. Odem (1992), CRRES plasma wave experiment, *J. Spacecr. Rockets, 29*, 570.

Baker, D. N. (2001) Satellite anomalies due to space storms, in *Space Storms and Space Weather Hazards*, edited by I. A. Daglis, 251, Springer, New York.

Baker, D. N., J. B. Blake, R. W. Klebesadel, and P. R. Higbie (1986), Highly relativistic electrons in the Earth's outer magnetosphere, 1. Lifetimes and temporal history 1979-1984, *J. Geophys. Res., 19*, 4265.

Baker, D. N., Blake, J. B., L. B. Callis, J. R. Cummings, D. Hovestadt, S. Kanekal, B. Blecker, R. A. Mewaldt, and R. D. Zwickl (1994), Relativistic electron acceleration and decay timescales in the inner and outer radiation belts: SAMPEX, *Geophys. Res. Lett., 21*, 409.

Baker, D. N. , X. Li, N. Turner, J. H. Allen, L. F. Bargatze, J. B. Blake, R. B. Sheldon, H. E. Spence, R. D. Belian, G. D. Reeves, S. G. Kanekal, B. Klecker, R. P. Lepping, K. W. Ogilvie, R. A. Mewaldt, T. Onsager, H. J. Singer, and G. Rostoker (1997), Recurrent geomagnetic storms and relativistic electron enhancements in the outer magnetosphere: ISTP coordinated measurements, *J. Geophys. Res., 102*, 14,141.

Baker, D. N., S. G. Kanekal, X. Li, S. P. Monk, J. Goldstein, and J. L. Burch (2004), An extreme distortion of the Van Allen belt arising from the Halloween solar storm in 2003, *Nature*, *432*, 878.

Blake, J. B., U. S. Inan, M. Walt, T. F. Bell, J. Bortnik, D. L. Chenette, and H. J. Christian (2001), Lightning-indiuced energetic electron flux enhancements in the drift loss cone, *J. Geophys. Res., 106*, 29,733.

Bortnik, J., U. S. Inan, and T. F. Bell (2003), Frequency-time spectra of magnetospherically reflecting whistlers in the plasmasphere, *J. Geophys. Res., 108*, 1030, doi:10.1029/2002JA009387.

Chan, K. W., and R. E. Holzer (1976), ELF hiss associated with plasma density enhancements in the outer magnetosphere, *J. Geophys. Res., 81*, 2267.

Chappell, C. R., K. K. Harris, and G. W. Sharp (1970), Morphology of bulge region of plasmasphere, *J. Geophys. Res., 75*, 3848.

Church, S., and R. M. Thorne (1983), On the origin of plasmaspheric hiss: ray path integrated amplification, *J. Geophys. Res., 88*, 7941.

Cornilleau-Wehrlin, N., R. Gendrin, F. Lefeuvre, M. Parrot, R. Grard, D. Jones, A. Bahnsen, E. Ungstrup, and W. Gibbons (1978), VLF electromagnetic waves observed onboard GEOS-1, *Space Sci. Rev.*, *22*, 371.

Cornilleau-Wehrlin, N., J. Solomon, A. Korth, and G. Kremser (1993), Generation mechanism of plasmaspheric ELF/VLF hiss: a statistical study from GEOS 1 data, *J. Geophys. Res., 98*, 21,471.

Dowden, R. L. (1971), Distinctions between mid latitude VLF hiss and discrete emissions, *Plant. Space Sci.*, *19*, 374.

Draganov, A. B., U. S. Inan, V. S. Sonwalker and T. F. Bell (1993), Magnetospherically-reflected whistlers as a source of plasmaspheric hiss, *Geophys. Res. Lett., 19*, 233.

Dunckel, N., and R. A. Helliwell (1969), Whistler mode emissions on the OGO 1 satellite, *J. Geophys. Res., 74*, 6731.

Glauert, S. A., and R. B. Horne (2005), Calculation of pitch angle and energy diffusion coefficients with the PADIE code, *J. Geophys. Res., 110*, A04206, doi:10.1029/2004JA010851.

Green, J. L., S. Boardsen, L. Garcia, W. W. Taylor, S. F. Fung, and B. W. Reinisch (2005), On the origin of whistler mode radiation in the plasmasphere, *J. Geophys. Res., 110*, A03201, doi:10.1029/2004JA010495.

Green, J. L., S. Boardsen, L. Garcia, W. W. Taylor, S. F. Fung, and B. W. Reinisch (2006), Reply to Comment on "On the origin of whistler mode radiation in the plasmasphere" by Green et al., *J. Geophys. Res., 111*, A09211, doi:10.1029/2006JA011622.

Gurnett, D. A. (1976), Plasma wave interactions with energetic ions near the magnetic equator, *J. Geophys. Res., 81*, 2765.

Gurnett, D. A., and R. R. Shaw 1973), Electromagnetic radiation trapped in the plasmasphere above the plasma frequency, *J. Geophys. Res., 78*, 8136.

Hayakawa, M., M. Parrot, and F. Lefeuvre (1986), The wave normals of ELF hiss emissions observed onboard GEOS 1 at the equatorial and off-equatorial regions of the plasmasphere, *J. Geophys. Res., 91*, 7989.

Horne, R. B. (1989) Path-integrated growth of electrostatic waves: The generation of terrestrial myriametric radiation, *J. Geophys. Res., 94*, 8895.

Horne, R. B. (2002), The contribution of wave particle interactions to electron loss and acceleration in the Earth's radiation belts during geomagnetic storms, in *Review of Radio Science 1999-2002*, Ed. W. R. Stone, Chapter 33, p801-828, John Wiley, Bognor Regis.

Horne, R. B., and R. M. Thorne (2003), Relativistic electron acceleration and precipitation during resonant interactions with whistler-mode chorus, *Geophys. Res. Lett., 30*, doi10.1029/2003GL016973.

Horne, R. B., R. M. Thorne, Y. Y. Shprits, N. P. Meredith, S. A. Glauert, A. J. Smith, S. G. Kanekal, D. N. Baker, M. J. Engebretson, J. L. Posch, M. Spasojevic, U. S. Inan, J. S. Pickett, and P. M. E. Decreau (2005), Wave acceleration of electrons in the Van Allen radiation belts, Nature, 437, 227, doi:10.1038/nature03939.

Horne, R. B., N. P. Meredith, S. A. Glauert, A. Varotsou, D. Boscher, R. M. Thorne, Y. Y. Shprits, and R. R. Anderson, Mechanisms for the acceleration of radiation belt electrons, in Co-rotating Solar Wind Streams and Recurrent Geomagnetic Activity, in

Geophys. Monogr. Ser., vol. 167, AGU, Washington, D. C., 2006

Huang, C. Y., C. K. Goertz, and R. R. Anderson (1983), A theoretical study of plasmaspheric hiss generation, *J. Geophys. Res., 88*, 7927.

Li, X., D. N. Baker, M. Temerin, T. E. Cayton, G. D. Reeves, R. A. Christiansen, J. B. Blake, M. D. Looper, R. Nakamura, and S. G. Kanekal (1997), Multi-satellite observations of the outer zone electron variation during the November 3-4, 1993, magnetic storm, *J. Geophys. Res., 102*, 14,123.

Lyons, L. R., and R. M. Thorne (1973), Equilibrium structure of radiation belt electrons, *J. Geophys. Res., 78*, 2142.

Lyons, L. R., R. M. Thorne, and C. F. Kennel (1972), Pitch angle diffusion of radiation belt electrons within the plasmasphere, *J. Geophys. Res., 77*, 3455.

Meredith, N. P., R. B. Horne, and R. R. Anderson (2001), Substorm dependence of chorus amplitudes: implications for the acceleration of electrons to relativistic energies, *J. Geophys. Res., 106*, 13,165.

Meredith, N. P., R. B. Horne, R. M. Thorne, D. Summers, and R. R. Anderson (2004), Substorm dependence of plasmaspheric hiss, *J. Geophys. Res., 109*, A06209, doi:1029/2004JA010387.

Meredith, N. P., R. B. Horne, S. A. Glauert, R. M. Thorne, D. Summers, J. M. Albert, and R. R. Anderson (2006a), Energetic outer zone electron loss timescales during low geomagnetic activity, *J. Geophys. Res., 101*, A05212, doi:10.1029/2005JA011516.

Meredith N. P., R. B. Horne, M. A. Clilverd, D. Horsfall, R. M. Thorne, R. R. Anderson (2006b), Origins of plasmaspheric hiss, *J. Geophys. Res., 111*, A09217, doi:10.1029/2006JA011707.

Parrot, M., and F. Lefeuvre (1986), Statistical study of the propagation characteristics of ELF hiss observed on GEOS 1, inside and outside the plasmasphere *Ann. Geophys.*, *4*, 363.

Paulikas, G. A., and J. B. Blake (1979), Effects of the solar wind on magnetospheric dynamics: energetic electrons at synchronous orbit, Quantitative modeling of magnetospheric processes, *Geophys. Monogr. Ser., 21*, edited by W. P. Olsen, AGU, Washington D.C., 180.

Reeves, G. D., R. H. W. Friedel, R. D. Belian, M. M. Meiet, M. G. Henderson, T. Onsager, H. J. Singer, D. N. Baker, X. Li, and J. B. Blake (1998), The relativistic electron response at geosynchronous orbit during the January 1997 magnetic storm, *J. Geophys. Res., 103*, 17,559.

Rodger, C. J., and M. A. Clilverd (2002), Inner radiation belt electron lifetimes due to whistler-induced electron precipitation (WEP) driven losses, *Geophys. Res. Lett., 29*, 1924, doi:10.1029/2002GL015795.

Russell, C. T., R. E. Holzer, and E. J. Smith (1969), OGO 3 observations of ELF noise in the magnetosphere, 1. Spatial extent and frequency of occurrence, *J. Geophys. Res., 74*, 755.

Santolik, O., M. Parrot, L. R. O. Storey, J. S. Pickett, and D. A. Gurnett (2001), Propagation analysis of plasmaspheric hiss using Polar PWI measurements, *Geophys. Res. Lett., 28*, 1127.

hprits Y. Y., R. M. Thorne, R. B. Horne, S. A. Glauert, M. Cartwright, C. T. Russell, D. N. Baker, S. G. Kanekal (2006), Acceleration mechanism responsible for the formation of the new radiation belt during the 2003 Halloween solar storm, Geophys. Res. Lett., 33, L05104, doi:10.1029/2005GL024256.

Singer, H. J., W. P. Sullivan, P. Anderson, F. Mozer, P. Harvey, J. Wygant, and W. McNeil, Fluxgate magnetometer instrument on the CRRES, *J. Spacecr. Rockets, 29*, 599, 1992.

Smith, E. J., A. M. Frandsen, B. T. Tsurutani, R. M. Thorne and K. W. Chan (1974), Plasmaspheric hiss intensity variations during magnetic storms, *J. Geophys. Res., 79*, 2507.

Smith, R. L. (1961), Propagation characteristics of whistlers trapped in field-aligned columns of enhanced ionisation, *J. Geophys. Res., 66*, 3699.

Solomon, J., N. Cornilleau-Wehrlin, A. Korth, and G. Kremser (1988), An experimental study of ELF/VLF hiss generation in the Earth's magnetosphere, *J. Geophys. Res., 93*, 1839.

Summers, D., C. Ma, and T. Mukai (2004) Competition between acceleration and loss mechanisms of relativistic electrons during geomagnetic storms, *J. Geophys. Res., 109*, A04221, doi:10.1029/2002JA009489.

Summers, D., B. Ni, and N. P. Meredith (2007a), Timescales for radiation belt acceleration and loss due to resonant wave particle interactions: 2. Evaluation for VLF chorus, ELF hiss and EMIC waves, *J. Geophys. Res.,* , in press.

Summers, D., B. Ni, and N. P. Meredith, R. B. Horne, R. M. Thorne, and R. R. Anderson (2007b), Electron scattering by whistler mode (ELF) hiss in plasmaspheric plumes, *J. Geophys. Res.,* , in preparation.

Thorne, R. M. and J. N. Barfield (1976), Further observational evidence regarding the origin of plasmaspheric hiss, *Geophys. Res. Lett., 3*, 29.

Thorne, R. M., and R. B. Horne (1994), Landau damping of magnetospherically reflected whistlers, *J. Geophys. Res., 99*, 17,249.

Thorne, R. M., E. J. Smith, R. K. Burton, and R. E. Holzer (1973), Plasmaspheric hiss, *J. Geophys. Res., 78*, 1581.

Thorne, R. M., E. J. Smith, K. J. Fiske, and S. R. Church (1974), Intensity variation of ELF hiss and chorus driving isolated substorms, *Geophys. Res. Lett., 1*, 193.

Thorne, R. M., S. R. Church, W. J. Malloy, and B. T. Tsurutani (1977), The local time variation of ELF emissions during periods of substorm activity, *J. Geophys. Res., 82*, 1585.

Thorne, R. M., S. R. Church, and D. J. Gorney (1979), On the origin of plasmaspheric hiss: the importance of wave propagation and the plasmapause, *J. Geophys. Res., 84*, 5241.

Thorne, R. M., R. B. Horne, S. A. Glauert, N. P. Meredith, Y. Y. Shprits, D. Summers, and R. R. Anderson (2005), The influence of wave-particle interactions on relativistic electrons during storms, in Inner Magnetosphere Interactions: New Perspectives From Imaging, in Geophys. Monogr. Ser., vol. 159, edited by J. Burch, M. Schulz, and H. Spence, AGU, Washington D.C., 2005.

Thorne, R. M., R. B. Horne, and N. P. Meredith (2006), Comment on "On the origin of whistler mode radiation in the plasmasphere" by Green et al., *J. Geophys. Res., 111*, A09210, doi:10.1029/2005JA011477.

Thorne, R. M., Y. Y. Shprits, N. P. Meredith, R. B. Horne, W. Li, S. Liu, L. R. Lyons, and R. R. Anderson (2007), Refilling of the slot region between the inner and outer electron radiation belts during geomagnetic storms, *J. Geophys. Res.,* , in press.

Voss, H. D., M. Walt, W. L. Imhof, J. Mobilia, and U. S. Inan (1998), Satellite observations of lightning-induced electron preciitation, *J. Geophys. Res., 103*, 11,725.

Wrenn, G. L. (1995), Conclusive evidence for internal dielectric charging anomalies on geosynchronous communications spacecraft, *J. Spacecraft and Rockets*, *32*, 514.

Wrenn, G. L., D. J. Rodgers, and K. A. Ryden (2002), A solar cycle of spacecraft anomalies due to internal charging, *Ann Geophys.*, *20*, 953-956.

Table 1. Gaussian Fits for Quiet Conditions

L	$f_{0,1}$	df_1	$B^2_{w,1}$	$f_{0,2}$	df_2	$B^2_{w,2}$	$f_{0,3}$	df_3	$B^2_{w,3}$
2.0	337	157	256	0.1	700	29	0.1	3090	3
2.5	343	169	651	0.1	650	54	0.1	1960	10
3.0	322	208	640	0.1	830	130	0.1	1810	5
3.5	262	256	600	0.1	640	140	0.1	1720	8
4.0	249	300	443	0.1	920	42	0.1	1990	6

Table 2. Gaussian Fits for Active Conditions

L	$f_{0,1}$	df_1	$B^2_{w,1}$	$f_{0,2}$	df_2	$B^2_{w,2}$	$f_{0,3}$	df_3	$B^2_{w,3}$
2.0	309	193	802	0.1	680	54	0.1	1960	5
2.5	293	302	2332	0.1	1200	61	0.1	2350	16
3.0	173	353	1867	0.1	1460	121	0.1	2480	46
3.5	209	210	1779	0.1	1130	531	0.1	2800	82
4.0	366	450	2199	0.1	1460	423	0.1	3030	161

Figure 1. Average wave intensities of plasmaspheric hiss (bottom) and lightning generated whistlers (top) as a function of L and MLT for different levels of geomagnetic activity. From left to right the results are presented for quiet ($AE^* < 100$ nT), moderate ($100 < AE^* < 500$ nT), and active ($AE^* > 500$ nT) conditions. The corresponding sampling distributions, color-coded to show the number of minutes in each (L, MLT) bin, t_b(m), are shown in the small panels.

Figure 2. Average wave spectral intensities (black) as a function of frequency for quiet (top) and active (bottom) conditions for $L = 2.0$ to $L = 4.0$ in steps of $0.5L$. The three Gaussian fits to each profile are coded red, orange and green.

Figure 3. Wave intensities of plasmaspheric hiss (red) and lightning generated whistlers (blue) as a function of L shell for quiet (left) and active (right) conditions. Plasmaspheric hiss intensities are plotted for $\psi_m = 0^o$ (solid), 52^o (dashed) and 80^o (dotted). Lightning generated wave intensities are shown for ducted whistlers (solid) and MR whistlers (dotted).

Table 3. Wave Normal Models

model	ψ	X_m	δX	X_{lc}	X_{uc}
small wave normal model	0.0	0.00	0.36	0.00	0.58
intermediate wave normal model	52.0	1.28	0.27	0.84	1.73
large wave normal model	80.0	5.67	2.74	1.43	11.4

Figure 4. (top) $f_{pe}/f_{ce,eq}$ as a function of L and MLT for different levels of geomagnetic activity. The corresponding sampling distributions, color-coded to show the number of minutes in each (L, MLT) bin, t_b(m), are shown in the small panels. (bottom) $f_{pe}/f_{ce,eq}$ as a function of MLT for selected L shells for different levels of geomagnetic activity. From left to right the results in the upper and lower panels are presented for quiet ($AE^* < 100$ nT), moderate ($100 < AE^* < 500$ nT), and active ($AE^* > 500$ nT) conditions. Line profiles (bottom) are shown for $L = 2.0$ (black), $L = 3.0$ (green) and $L = 4.0$ (red). The colour coded dotted lines represent the average values used to determine the loss timescales.

Figure 5. $f_{pe}/f_{ce,eq}$ versus L shell for quiet(blue) and active(red) conditions.

Figure 6. Electron loss timescales due to plasmaspheric hiss (red) and lightning generated whistlers (blue) as a function of energy at $L = 2.5$ during active conditions. Loss timescales are shown for plasmaspheric hiss propagating at small (solid), medium (dashed), and large (dotted) wave normal angles and for ducted (solid) and MR (dashed) whistlers.

Figure 7. Electron loss timescales due to plasmaspheric hiss (red) and lightning generated whistlers (blue) as a function of energy. The results are presented for quiet conditions (top) and active conditions (bottom) for $L = 2.0$ to $L = 4.0$ in steps of $0.5L$. Loss timescales are shown for plasmaspheric hiss propagating at small (solid), medium (dashed), and large (dotted) wave normal angles and for ducted (solid) and MR (dashed) whistlers.

Figure 8. Electron loss timescales due to plasmaspheric hiss (red) and lightning generated whistlers (blue) as a function of L shell. The results are presented for quiet (top) and active (bottom) conditions for 100 keV $< E <$ 2 MeV. Loss timescales shown for plasmaspheric hiss propagating at small (solid), medium (dashed), and large (dotted) wave normal angles and for ducted (solid) and MR (dashed) whistlers.

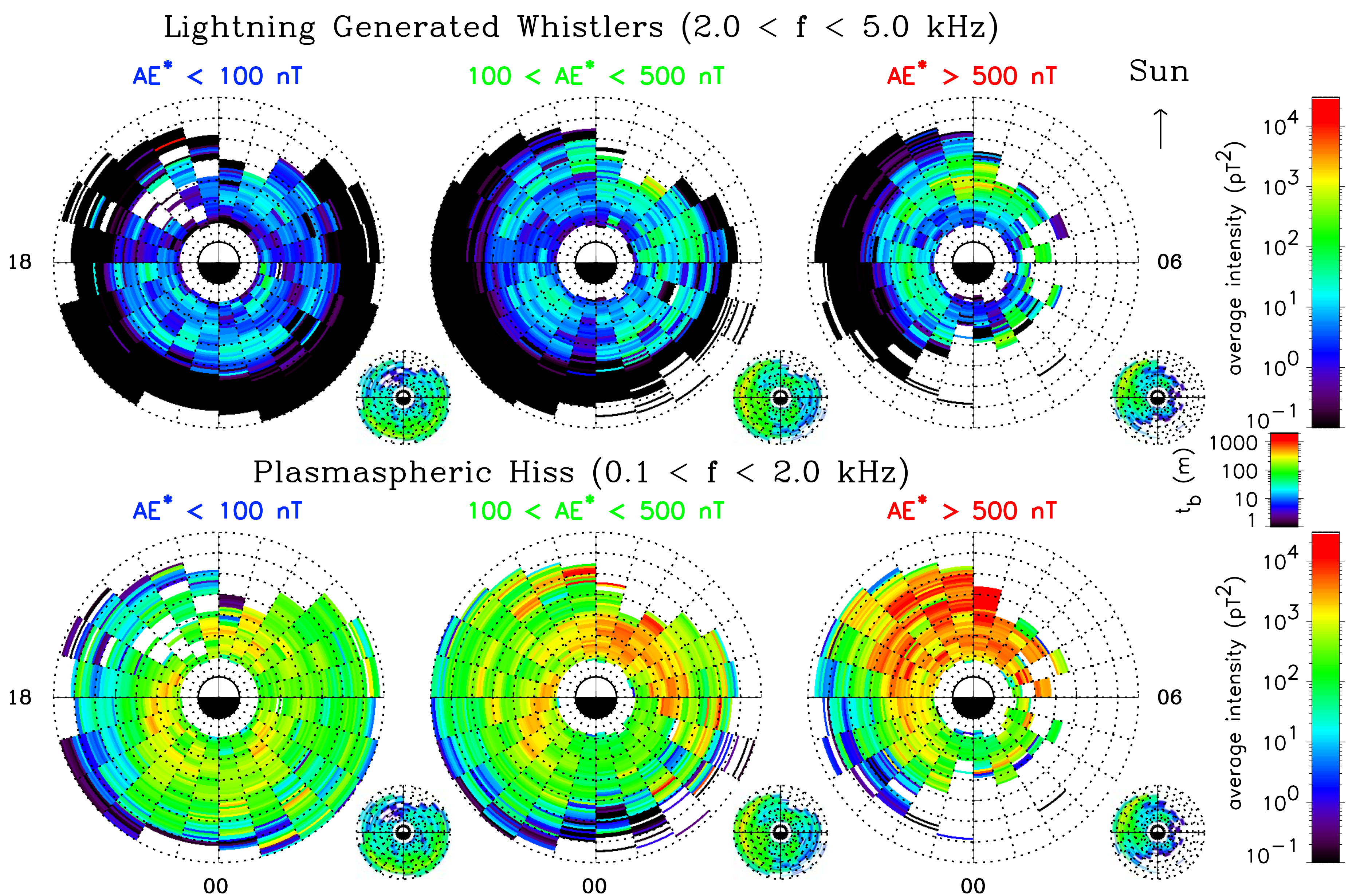

Lightning Generated Whistlers (2.0 < f < 5.0 kHz)
AE* < 100 nT
100 < AE* < 500 nT
AE* > 500 nT
Sun
18
06
00
average intensity (pT2)
t_b (m)
1000
100
10
1
Plasmaspheric Hiss (0.1 < f < 2.0 kHz)

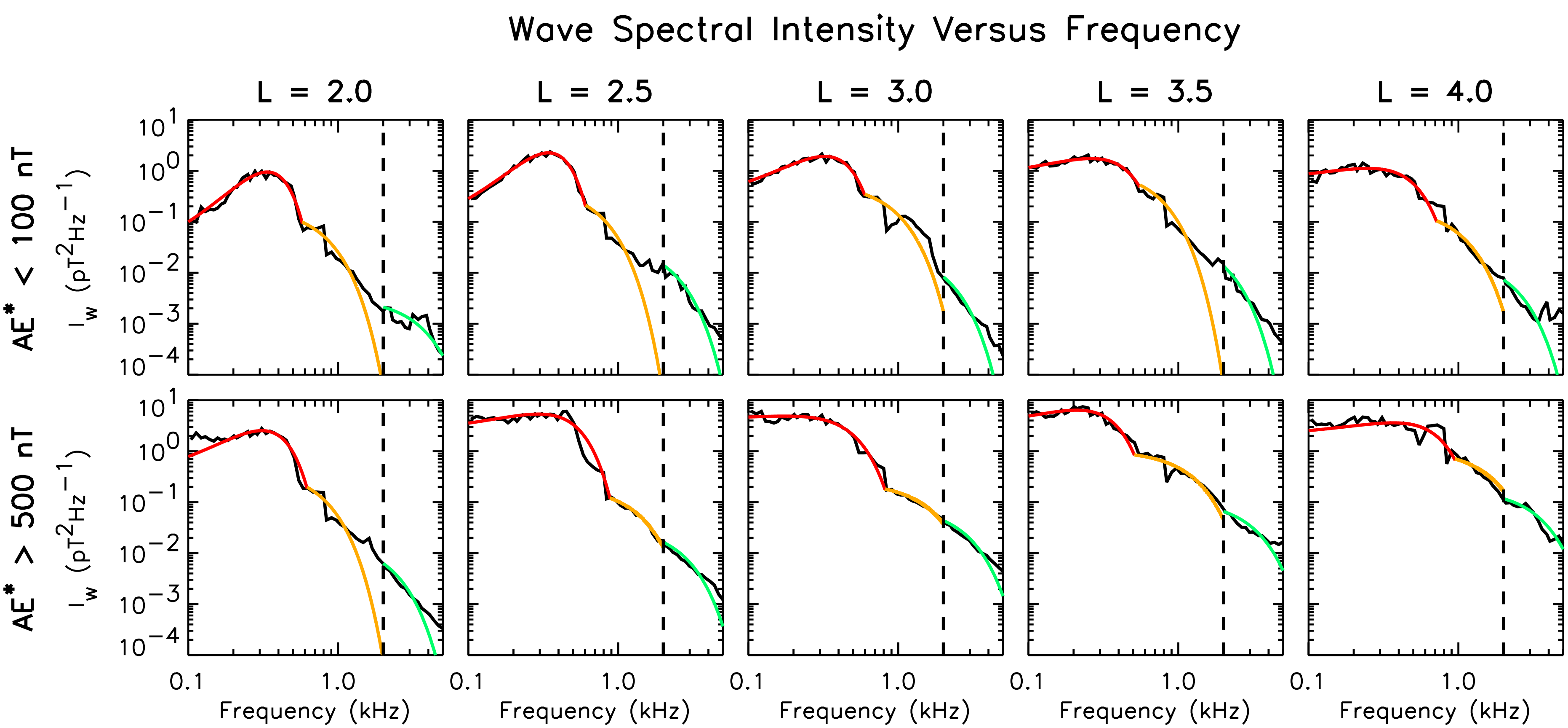

Wave Spectral Intensity Versus Frequency
L = 2.0
L = 2.5
L = 3.0
L = 3.5
L = 4.0
AE* < 100 nT
AE* > 500 nT
I_w (pT^2Hz^-1)
Frequency (kHz)

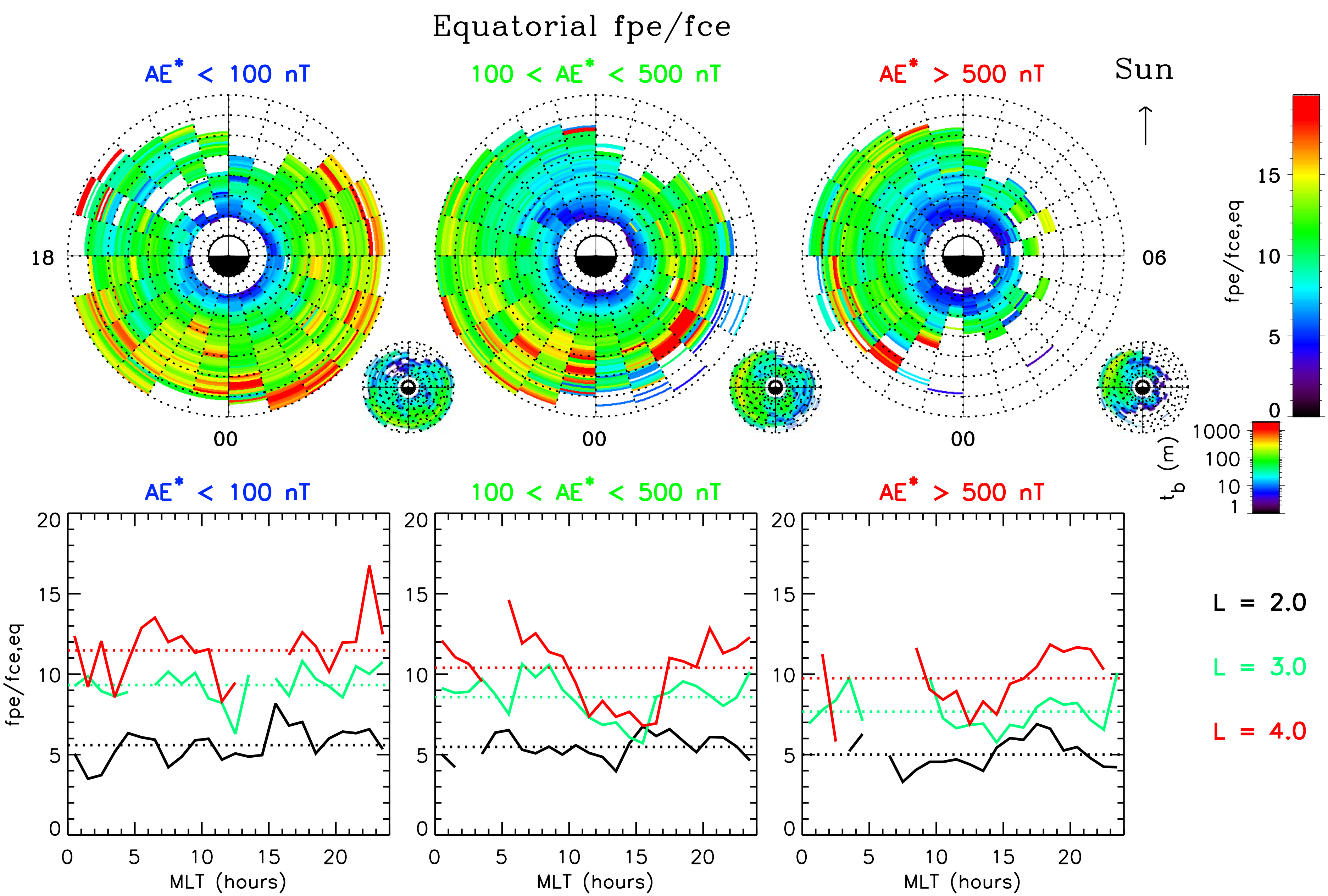

Equatorial fpe/fce
AE* < 100 nT
100 < AE* < 500 nT
AE* > 500 nT
Sun
18
06
00
fpe/fce,eq
0
5
10
15
t_b (m)
1
10
100
1000
fpe/fce,eq
MLT (hours)
0
5
10
15
20
L = 2.0
L = 3.0
L = 4.0

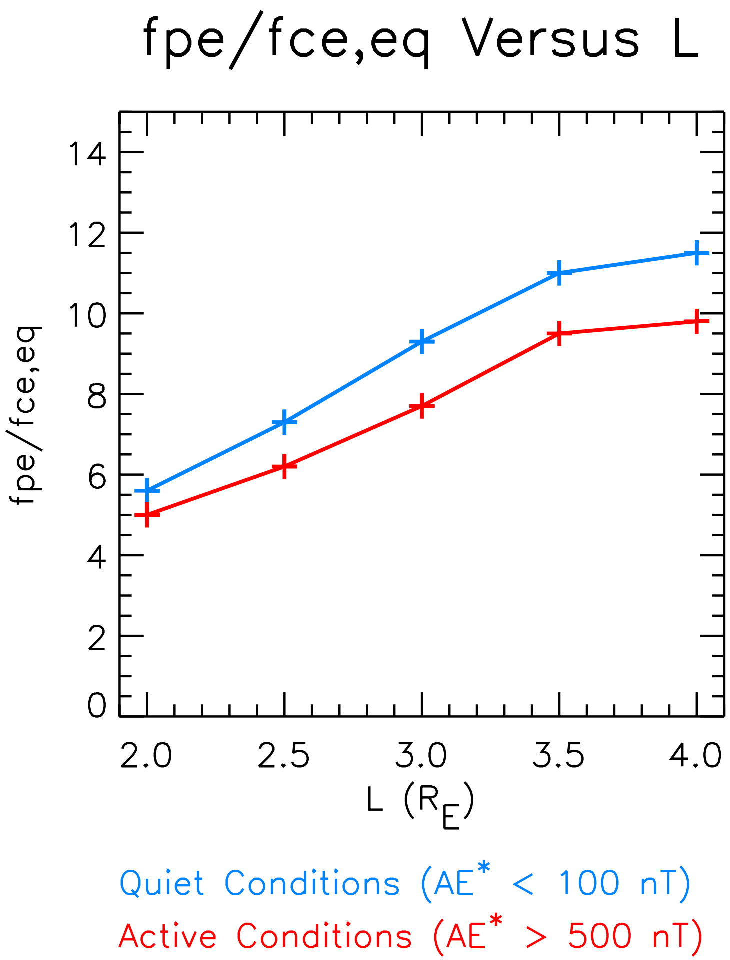
fpe/fce,eq Versus L
fpe/fce,eq
0
2
4
6
8
10
12
14
2.0
2.5
3.0
3.5
4.0
L (RE)
Quiet Conditions (AE* < 100 nT)
Active Conditions (AE* > 500 nT)

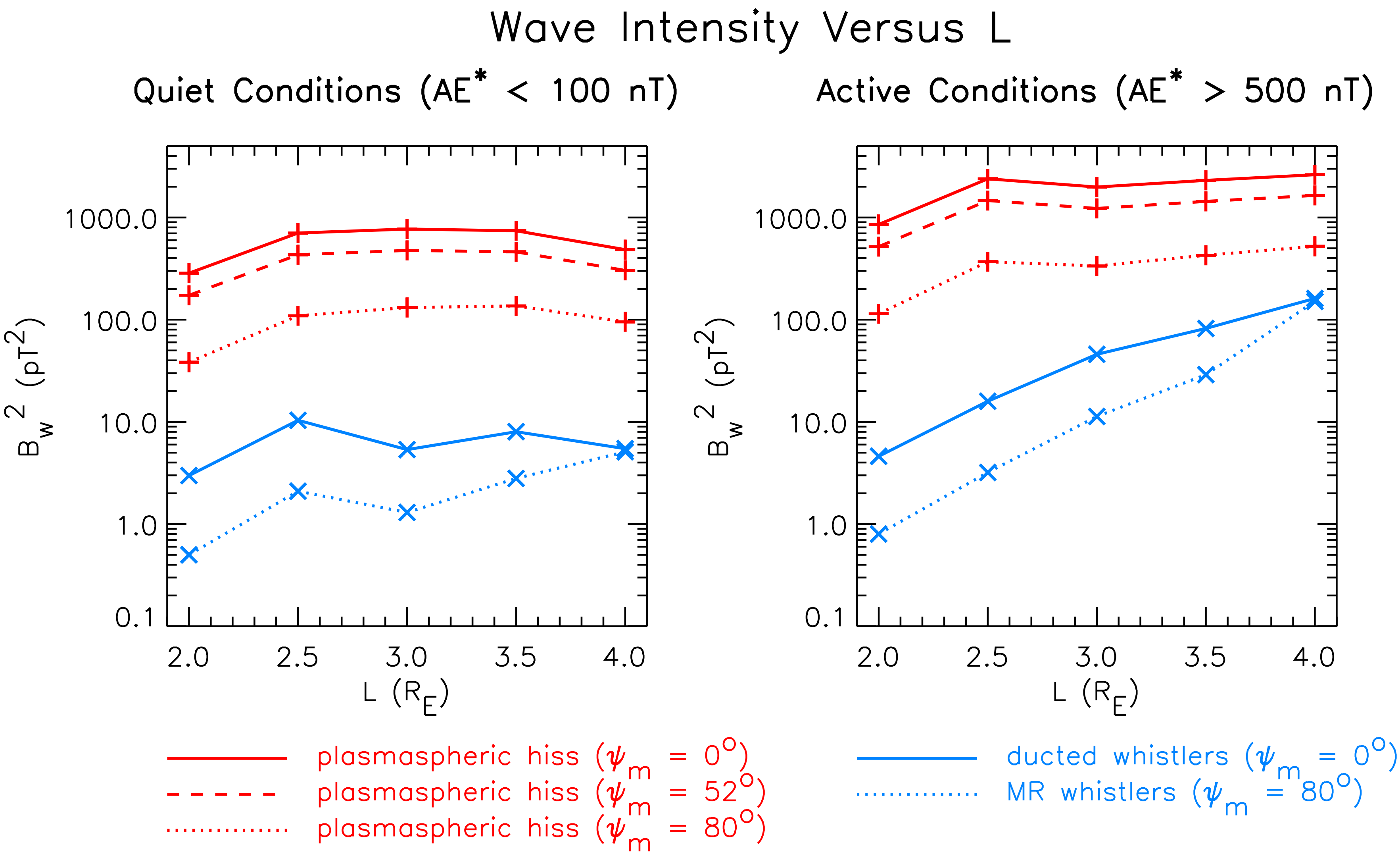
Wave Intensity Versus L
Quiet Conditions (AE* < 100 nT)
Active Conditions (AE* > 500 nT)
B_w^2 (pT^2)
1000.0
100.0
10.0
1.0
0.1
2.0
2.5
3.0
3.5
4.0
L (R_E)
plasmaspheric hiss (ψ_m = 0°)
plasmaspheric hiss (ψ_m = 52°)
plasmaspheric hiss (ψ_m = 80°)
ducted whistlers (ψ_m = 0°)
MR whistlers (ψ_m = 80°)

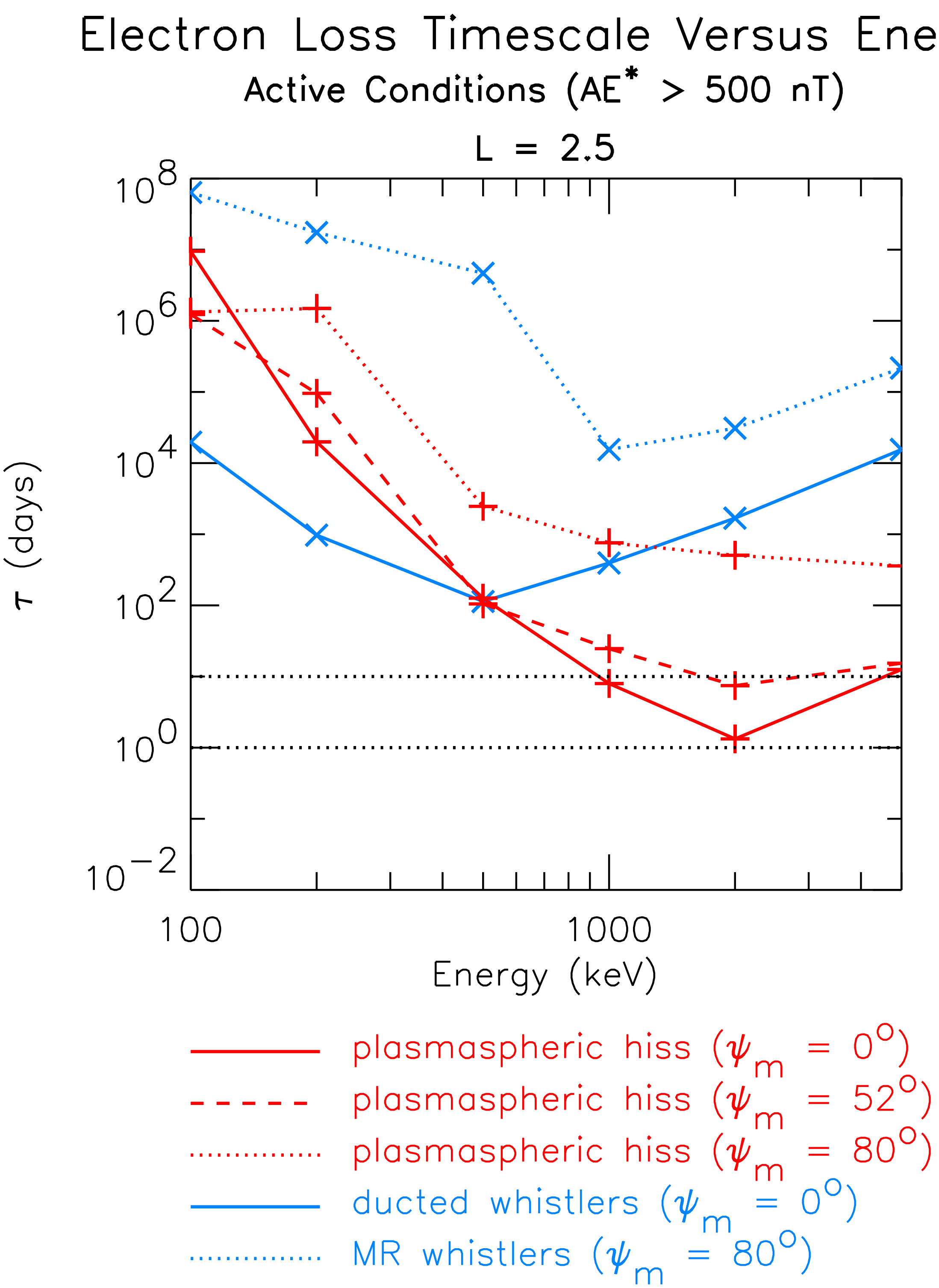

Electron Loss Timescale Versus Energy
Active Conditions (AE* > 500 nT)
L = 2.5
10^8
10^6
10^4
10^2
10^0
10^{-2}
τ (days)
100
1000
Energy (keV)
plasmaspheric hiss (ψ_m = 0°)
plasmaspheric hiss (ψ_m = 52°)
plasmaspheric hiss (ψ_m = 80°)
ducted whistlers (ψ_m = 0°)
MR whistlers (ψ_m = 80°)

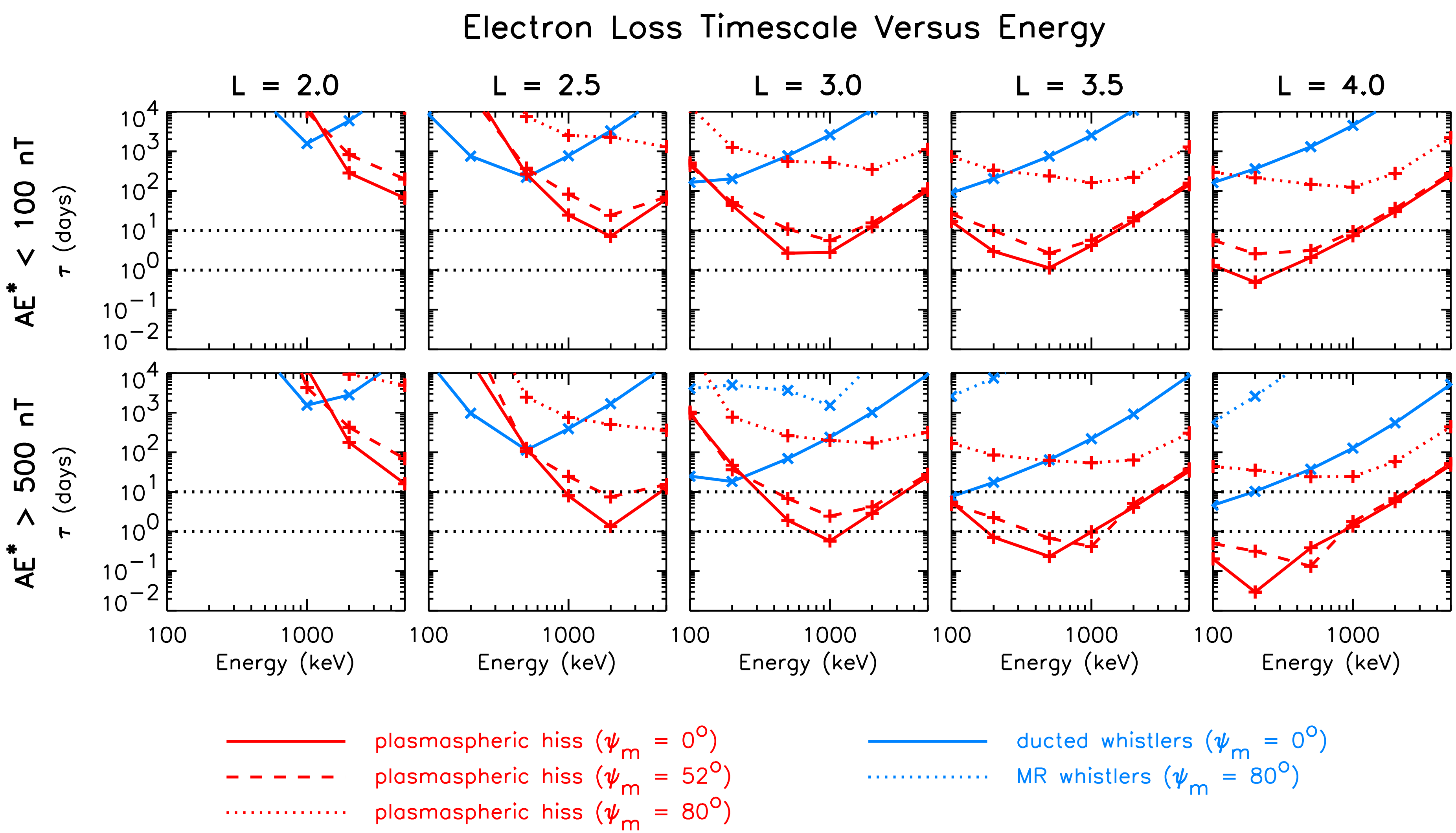

Electron Loss Timescale Versus Energy
L = 2.0
L = 2.5
L = 3.0
L = 3.5
L = 4.0
AE* < 100 nT
AE* > 500 nT
τ (days)
Energy (keV)
plasmaspheric hiss (ψm = 0°)
plasmaspheric hiss (ψm = 52°)
plasmaspheric hiss (ψm = 80°)
ducted whistlers (ψm = 0°)
MR whistlers (ψm = 80°)

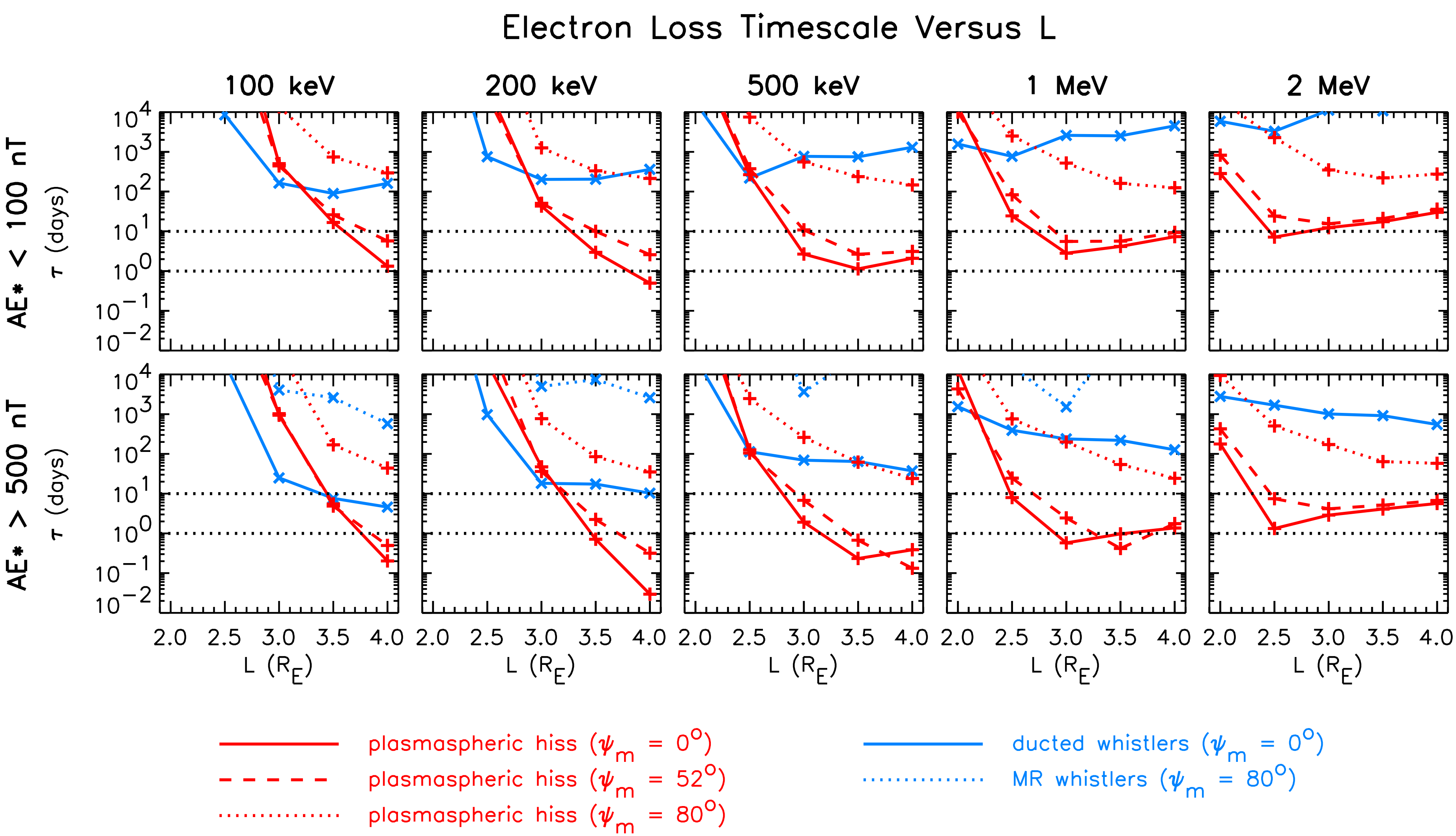

Electron Loss Timescale Versus L
100 keV
200 keV
500 keV
1 MeV
2 MeV
AE* < 100 nT
AE* > 500 nT
τ (days)
L (R_E)
plasmaspheric hiss (ψ_m = 0°)
plasmaspheric hiss (ψ_m = 52°)
plasmaspheric hiss (ψ_m = 80°)
ducted whistlers (ψ_m = 0°)
MR whistlers (ψ_m = 80°)